Mechanical and Rheological Properties, and Morphology of Polyamide-6/Organoclay/Elastomer Nanocomposites

Isil Isik-Gulsac, Ulku Yilmazer, Goknur Bayram

Chemical Engineering Department, Middle East Technical University, Ankara 06800, Turkey

Received 21 June 2011; accepted 5 January 2012
DOI 10.1002/app.36746
Published online in Wiley Online Library (wileyonlinelibrary.com).

ABSTRACT: The effects of ethylene-methyl acrylate-glycidyl methacrylate (E-MA-GMA) terpolymer and three types of organoclays (Cloisite® 15A, 25A, and 30B) on mechanical and rheological properties, and morphology of impact modified polyamide-6/montmorillonite ternary nanocomposites were investigated by X-ray diffraction (XRD), transmission electron microscopy (TEM), scanning electron microscopy (SEM), parallel disk rheometry, melt flow index measurements, and tensile and impact tests. The materials were prepared by melt blending using a co-rotating twin-screw extruder. XRD and TEM analyses showed that exfoliated-intercalated nanocomposites were formed in both polyamide-6/Cloisite® 25A and Cloisite® 30B binary nanocomposites and in ternary systems. SEM micrographs showed that rubber domain sizes were larger in the nanocomposites than in their corresponding polyamide-6/elastomer blends. Generally, tensile strength, Young's modulus, and elongation at break decreased with the addition of elastomer to polyamide-6/organoclay binary nanocomposites. In the melt state, liquid-like behavior of polyamide-6 slightly turned to pseudo solid-like in the binary and ternary nanocomposites. © 2012 Wiley Periodicals, Inc. J Appl Polym Sci 000: 000–000, 2012

Key words: nanocomposites; polyamides; elastomers; mechanical properties; rheology

INTRODUCTION

Polyamide-6 nanocomposites find many industrial applications in automotive industry, food packaging, medicals, and many other fields. They show superior strength, modulus, heat distortion temperature, and water and gas barrier properties in comparison to pure polyamide-6.[1–3] However, notch sensitivity and ductile–brittle transition temperature sharply increase as montmorillonite content is increased.[4] High toughness can be achieved by incorporating a low modulus, reactive or non-reactive, rubbery-type component to the polymer matrix. Thus, rubber toughening of polyamide-6-based nanocomposites is performed to expand the areas of application. Most of the studies are focused on toughening these nanocomposites with elastomers having maleic anhydride functional groups.[5–11]

Polyamide-6/maleated polypropylene blend based nanocomposites were studied by Chow et al.[12–14] Nanocomposite morphology, and mechanical, thermal, and dynamic mechanical properties were investigated. Clay surface was modified by octadecylamine, and it was claimed that hydrogen bonding between amine groups of octadecylamine in the intercalant of clay and carbonyl groups of polyamide-6 and polyamide-6-*g*-polypropylene favored exfoliation. Khatua et al.[15] investigated the effects of organoclay platelets on morphology of polyamide-6 and ethylene propylene rubber (EPR) blends by scanning electron microscopy (SEM) and transmission electron microscopy (TEM). It was observed that, domain size of EPR dispersed phase in blends containing 20 wt % EPR decreased significantly, even if a small amount of organoclay was added. Their results indicated that if the clay becomes exfoliated in the polymer matrix, the exfoliated clay platelets prevent the coalescence of the dispersed domains. Chiu et al.[16] prepared polyamide-6 and maleated polyolefin elastomer (POEMA) based nanocomposites using one type of commercial organoclay. Their X-ray diffraction (XRD) results showed that both organoclay and polyolefin elastomer induce the formation of γ form of crystal. Storage modulus, Young's modulus, and tensile strength increased after the addition of organoclay. However, these properties declined after further incorporation of elastomer. Maleated styrene-ethylene/butylene-styrene triblock copolymer (SEBS-MA) (up to 40 wt %) toughened polyamide-6 nanocomposites with 3 wt % organoclay were studied by González et al.[17] The morphology of polyamide-6 matrix did not

Correspondence to: I. Isik-Gulsac (isil.gulsac@mam.gov.tr).
Contract grant sponsor: Scientific and Technological Research Council of Turkey (TUBITAK); contract grant number: 104M415.

change upon blending with elastomer. However, sizes of rubber particles in nanocomposites were larger than in their corresponding blends. Supertough nanocomposites were obtained with 30 wt % SEBS-MA. In another study, the effects of clay loading on morphology and mechanical properties of the same material combinations were investigated.[18] The elastomer content was selected as 30 wt %. The interactions between the organoclay surfactant and elastomer maleic anhydride groups led to a decrease in compatibility, and the particle size was smaller. Nishitani et al.[19] studied the effects of addition of functionalized styrene-ethylene/butylene-styrene (SEBS) on dynamic viscoelastic, mechanical, and tribological properties of polyamide-6 nanocomposites. Four types of SEBS (unmodified SEBS, maleic anhydride grafted SEBS, amine group grafted SEBS, and carboxyl group grafted SEBS) were added to polyamide-6/clay nanocomposite to prepare various nanocomposites. The viscoelastic properties were found to increase with the addition of SEBS and were highly affected by the types of functionalized groups present. The mechanical and viscoelastic properties correlated closely with the size of dispersed SEBS domains and interparticle distance. Kelnar et al.[20] examined the morphology and mechanical properties of polyamide-6/organoclay ternary nanocomposites prepared by different types of both reactive and non-reactive elastomers, such as maleated ethylene propylene elastomer (EPR-MA), EPR, SEBS-MA, SEBS, ethylene-methyl acrylate-glycidyl methacrylate (E-MA-GMA), ethylene-methyl acrylate (E-MA), and poly(acrylonitrile-*co*-butadiene) rubber (NBR). The effects of clay content and elastomer type were investigated. It was observed that mechanical properties of the system were influenced by elastomer type and particle size, clay localization and its degree of ordering. Kelnar et al.[21] investigated the effects of clay treatment on structure and mechanical behavior of polyamide-6 nanocomposite containing elastomer. Four different types of elastomers such as EPR-MA, EPR, E-MA, and hydrogenated NBR were used. It was shown that the modification of clay simultaneously affected the degree of polyamide-6 matrix reinforcement, and the size and structure of dispersed EPR.

In order to understand the effects of various shear histories on polymer nanocomposite systems, rheological behavior of nanocomposites were also studied in the literature.[4,14,22–25]

There are no studies investigating the effects of organoclay surfactant type on the rheological properties of polyamide-6/organoclay/elastomer ternary nanocomposites. Rheological characterization of the polyamide-6-based ternary nanocomposites is very important, since viscoelastic measurements are highly sensitive to the nanoscale structure of the hybrids and appear to be a powerful method to probe the developed structure of such materials.

In this study, the effects of reactive E-MA-GMA terpolymer and organoclay type on mechanical and rheological properties, and morphology of the impact modified polyamide-6/montmorillonite ternary nanocomposites were investigated by XRD, TEM, SEM, parallel disk rheometry, melt flow index (MFI) measurements, and tensile and impact tests. Polyamide-6 has good overall mechanical properties; and ethylene terpolymer is used to provide high resistance against moisture, to improve low temperature behavior and it ensures good processability. It is possible that these two polymers be compatible through reactive GMA functional group in elastomer and functional groups of polyamide-6.

MATERIALS AND EXPERIMENTAL

Materials

The polymer matrix, polyamide-6 (Teklamid) with a density value of 1.13 g/cm^3 at 25°C (ISO 1183) was obtained from Polyone Tekno Polimer Company (Turkey) as pellets. The elastomeric material; Lotader 8900, E-MA-GMA terpolymer was purchased from Arkema Chemicals (France). The ester and glycidyl methacrylate contents were 25 wt % and 8 wt %, respectively.

The layered silicates used in this study were montmorillonites Cloisite® 15A, Cloisite® 25A, and Cloisite® 30B from Southern Clay Products, Inc. (Gonzales, Texas USA) that were produced by the manufacturer by a cation exchange reaction between sodium montmorillonite and various quaternary alkyl ammonium salts. Cloisite® 15A is modified by dimethyl, dihydrogenated tallow quaternary ammonium at a concentration of 125 meq/100 g clay. Cloisite® 25A is modified by dimethyl, hydrogenated tallow, 2-ethyl hexyl quaternary ammonium at a concentration of 95 meq/100 g clay. Cloisite® 30B is modified by methyl, tallow, bis-2-hydroxyethyl, quaternary ammonium at a concentration of 90 meq/100 g clay. According to the manufacturer's data, surface hydrophobicity is the highest in Closite® 15A and the least in 30B. Cloisite® 25A is in between them. Table I shows the molecular structures of organic modifiers that were used in this study.

Nanocomposite preparation

Organically treated montmorillonite (2 wt %), elastomer (5 wt %), and polyamide-6 nanocomposites were prepared by melt compounding in a Thermoprism TSE 16 TC, co-rotating, intermeshing twin-screw extruder ($D = 16$ mm, $L = 384$ mm) at a screw speed of 250 rpm, at a feed rate of 25 g/min. The

TABLE I
Molecular Structures of the Organic Modifiers

Cloisite® 15A	Cloisite® 25A	Cloisite® 30B
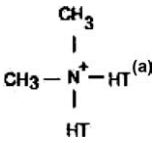	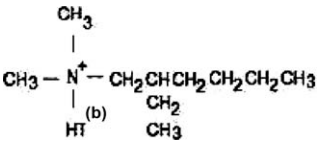	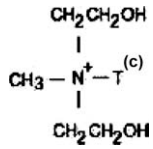

[a] HT is hydrogenated tallow (~ 65% C18; ~30% C16; ~5% C14), anion: chloride.
[b] HT is hydrogenated tallow (~ 65% C18; ~30% C16; ~5% C14), anion: methyl sulfate.
[c] T is tallow (~ 65% C18; ~30% C16; ~5% C14), anion: chloride.

temperature profile of the barrel was 220–240–240–240–240°C from the hopper to the die. Prior to compounding, polyamide-6, organically modified montmorillonites and the elastomeric material were dried under vacuum.

The dry-blended pellets of polyamide-6 and elastomer were fed from the main feeder and the organoclay particles were fed to the extruder simultaneously by a second feeder from the main feed port. In order to maximize the interactions between polyamide-6, elastomer, and organoclays, all components were extruded simultaneously. Pellets obtained from the extrusion were dried and fed to the extruder from the main feeder and extruded once more. In addition to the ternary nanocomposites, binary polyamide-6/organoclay nanocomposites and polyamide-6/elastomer blends were also melt compounded using a similar procedure to investigate the effects of clay and elastomer. In addition, pure polyamide-6 was also extruded twice for comparison.

Dry-extruded pellets were injection molded (Microinjector, Daca Instruments, Santa Barbara, California USA) according to ASTM 638-M91-a at barrel temperature of 240°C and mold temperature of 30°C. After injection molding, the samples were immediately sealed in polyethylene bags and stored in vacuum desiccators for at least 24 h prior to testing.

Characterization experiments

X-ray diffraction pattern of the Cloisite Na^+ (pure montmorillonite) was recorded by monitoring the diffraction angle 2θ from 1° to 10° on a Rigaku Geigerflex diffractometer using CuKα, radiation source at a generator voltage of 40 kV, and a generator current of 30 mA. The scanning speed and the step size used were at 2°/min and 0.02°, respectively. The organoclays and composites were analyzed by using a RIGAKU D/MAX 2200/PC X-ray diffractometer. CuKα (λ = 1.54 Å) radiation, generated at a voltage of 40 kV and current of 40 mA, was used as the X-ray source. The diffraction angle 2θ was scanned from 1° to 10° at a scanning rate of 1°/min and a step size of 0.01°. Philips CM200 TEM at an acceleration voltage of 120 kV was used to examine the samples. Ultra-thin sections of 70 nm in thickness were cryogenically cut with a diamond knife at a temperature of −100°C. All samples were trimmed parallel to the injection molding direction. The fracture surfaces of the materials obtained by impact testing were examined by a low voltage SEM (JEOL JSM-6400). Polyethylene-based elastomeric material phase was selectively etched in hot xylene for the SEM analysis and then coated with gold. Domain sizes of 100–250 etched elastomer regions were analyzed by Image J software (Image Processing and Analysis in Java) by NIH. MFI measurements were carried out according to ASTM D1238-79 using Omega Melt Flow Indexer (Turkey). The temperature and load were selected as 235°C and 2.16 kg, respectively. Tensile tests were performed using a computer controlled testing machine (Lloyd 30K), according to ASTM 638-M 91a. The strain rate was 0.1 min^{-1}. Notched charpy impact strength was measured using Ceast Resil Impactor (Akron, Ohio USA) according to ISO-179. All mechanical tests were performed at 23°C. Tensile and impact properties reported represent the average of the results on at least five samples. Dynamic rheological measurements were performed by 25 mm diameter parallel disks in oscillatory shear mode using a scientific rotational rheometer (ARES-Advanced Rheometric Expansion System, TA Instruments, New Castle, Delaware USA). For rheological analysis, extruded pellets were compression molded at 250°C, for 4 min in order to obtain disks having diameter of 25 mm and thickness of 1 mm. For polyamide-6/Cloisite® 25A/E-MA-GMA nanocomposite, strain amplitude was swept from 1 to 20% at 240°C at 5 rad/s angular frequency, and the storage modulus, loss modulus, and complex viscosity versus percentage strain were obtained. These values remained constant in the studied strain range. Thus, in the analysis that followed, 5% strain amplitude was selected to ensure that the experiments were performed in linear viscoelastic region. Dynamic storage modulus, G', dynamic loss modulus, G'', and complex viscosity, η^* were recorded as functions of angular frequency, ω, at 240°C. The frequency test range was from 1 to 100 rad/s. The experiments were conducted under nitrogen atmosphere in order to prevent oxidative degradation.

RESULTS AND DISCUSSION

X-ray analysis

Figure 1(a) shows the XRD pattern of pure unmodified montmorillonite Cloisite® Na^+, whereas Figure 1(b) shows XRD patterns of pure Cloisite® 15A,

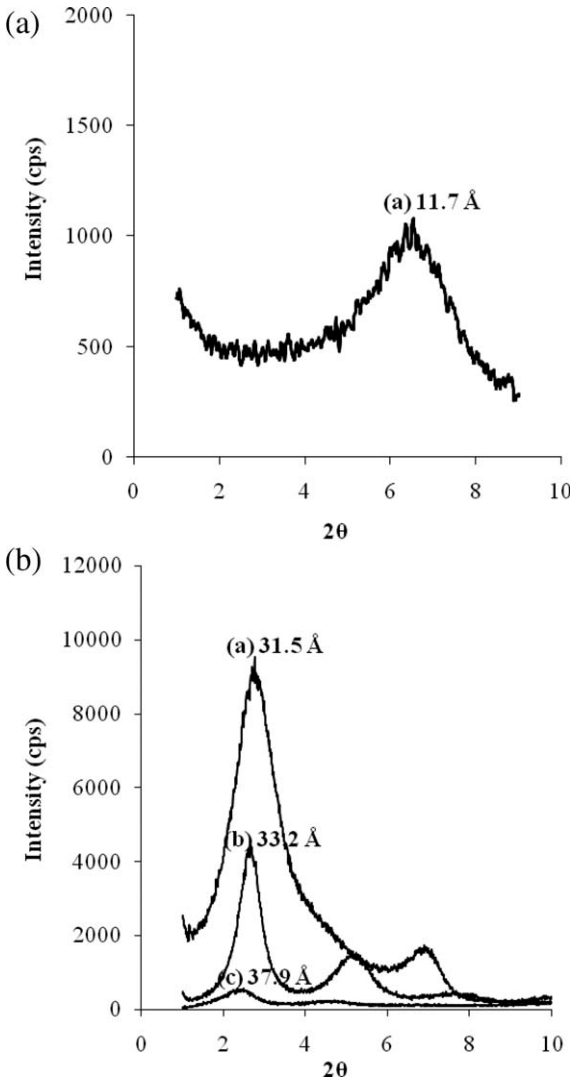

Figure 1 (a) XRD pattern for Cloisite® Na^+. (b) XRD patterns for (a) Cloisite® 15A, (b) polyamide-6/Cloisite® 15A nanocomposite, and (c) polyamide-6/Cloisite® 15A/E-MA-GMA nanocomposite.

polyamide-6/Cloisite® 15A binary nanocomposite, and polyamide-6/Cloisite®15A/E-MA-GMA ternary nanocomposite. Table II shows the *d*-spacing data of these samples calculated by using Bragg's equation from the first (d_{001}) and second (d_2) diffraction peaks in the figure. (The term d_2 does not refer to diffraction from the second plane. It just denotes the second peak observed in the XRD data). XRD diffractogram of Cloisite® Na^+ reveals only a d_{001} peak corresponding to basal spacing of 11.7 Å. XRD diffractogram of Cloisite® 15A organoclay shows two diffraction peaks. The second peak may result from a second silicate layer if 2θ is approximately twice the value of the first characteristic peak of the clay, or it may be due to a reflection from a portion of the clay where the inorganic cations of the smectite clay are not fully replaced by the organic ions if 2θ is approximately the same as 2θ for unmodified clay.[26,27] In the 2θ = 1–10° interval, polyamide-6 shows no peaks. It can be seen from Figure 1(b) that, the *d*-spacing calculated from d_{001} diffraction peak, did not significantly change when Cloisite® 15A was melt blended with polyamide-6, whereas in nanocomposites containing polyamide-6 and E-MA-GMA elastomer, d_{001} *d*-spacing increased from 31.5 Å to 37.9 Å. The d_2 *d*-spacing of Cloisite® 15A in powder form corresponds approximately to the d_{001} *d*-spacing of pure montmorillonite which is not modified by the quaternary ammonium salt.[28] It is observed that, d_2 peak is shifted to lower angles when Cloisite® 15A is compounded with polymers indicating that a few polymer chains are intercalated between the clay layers. Initial d_2 interlayer spacing of pure Cloisite® 15A (12.8 Å) is increased to 17.0 Å and 18.1 Å when it is compounded with polyamide-6 and polyamide-6/elastomer blend, respectively. Thus, it is thought that d_2 *d*-spacing in nanocomposites is observed by intercalation of polymer into unmodified clay layers. This is supported by the fact that the peak at 12.8 Å is not observed in the nanocomposites.

It is seen from Figure 1(b) that intensity of both the first and second peaks of pure organoclay 15A decreases, indicating transformation of large silicate agglomerates into small tactoids as a result of increased viscosity and shear intensity. Extrusion of polymer matrix twice helped overcome the cohesive forces between the clay layers by the hydrodynamic separation forces of the polymer matrix and provided easier diffusion of polymer chains into the organoclay gallery. Decrease in intensity can be associated with the decrease in the number of layers of individual clay particles.[29]

Figure 2 shows the XRD patterns of pure Cloisite® 25A, binary nanocomposite containing polyamide-6/Cloisite® 25A, and ternary nanocomposite of polyamide-6/Cloisite® 25A/E-MA-GMA. The organoclay XRD pattern exhibits an intense peak at around 2θ = 4.75° corresponding to basal spacing of 18.6 Å. The XRD patterns of binary as well as ternary nanocomposites show that the characteristic peak of the pure organoclay is shifted to lower angles, indicating that

TABLE II
***d*-Spacing Data of Polyamide-6/Cloisite® 15A Based Nanocomposites**

	d_{001} *d*-spacing (Å)	d_2 *d*-spacing (Å)
Pure Cloisite Na^+ in powder form	11.7	–
Pure Cloisite® 15A in powder form	31.5	12.8
Polyamide-6 + Cloisite® 15A	33.2	17.0
Polyamide-6 + Cloisite® 15A + E-MA-GMA	37.9	18.1

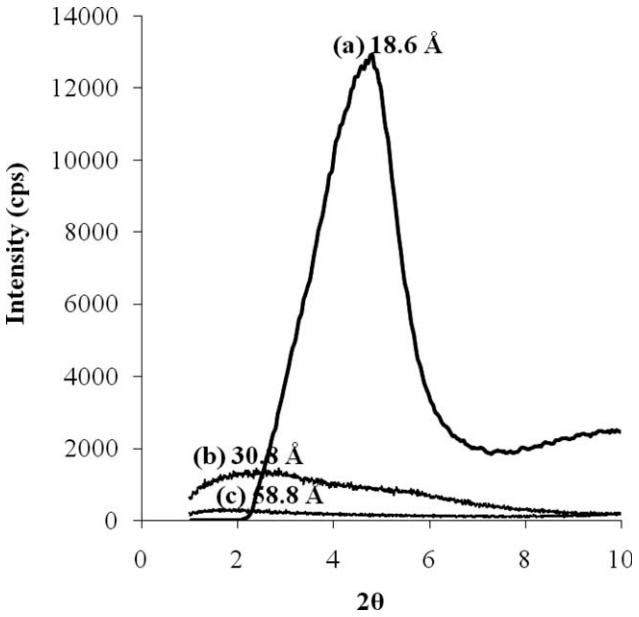

Figure 2 XRD patterns for (a) Cloisite® 25A, (b) polyamide-6/Cloisite® 25A nanocomposite, and (c) polyamide-6/Cloisite® 25A/E-MA-GMA nanocomposite.

the polymer chains are intercalated between the clay galleries. For intercalated nanocomposites, the expansion associated with the polymer intercalation results in the appearance of a new basal reflection corresponding to larger gallery height, which is 30.8 Å (65.6% increase) and 58.8 Å (216.3% increase) for polyamide-6/Cloisite® 25A and polyamide-6/Cloisite® 25A/E-MA-GMA nanocomposites, respectively. Also, as it can be seen in Figure 2, the peaks of the organoclay in both nanocomposites are very broad. This, along with the TEM data shown later, indicates that the organoclay used is partly intercalated and partly exfoliated, both in the presence of pure polyamide-6 and E-MA-GMA.

Figure 3 shows the XRD spectra of pure Cloisite® 30B, binary nanocomposite containing polyamide-6/Cloisite® 30B, and ternary nanocomposite of polyamide-6/Cloisite® 30B/E-MA-GMA. Organoclay *d*-spacing is increased from 18.5 Å to approximately 41.4 Å (123.8% increase) and 45.9 Å (148.1% increase) when the organoclay is melt blended with polyamide and impact modified polyamide-6, respectively. Similar to Figure 2, XRD patterns for these nanocomposites exhibit very broad peaks indicating that partially intercalated and partially exfoliated nanocomposites are obtained.

High degree of dispersion of Cloisite® 30B in nanocomposites can be attributed to the existence of possible reaction between the hydroxyl group of Cloisite® 30B and the carboxyl group of polyamide-6, as well as to hydrogen bonding between the surfaces of the two. Mohamadi et al.[30] prepared polyamide-6/organoclay nanocomposites by *in-situ* polymerization and investigated crystalline and thermal properties of the samples. Their FTIR studies indicated that some of the polyamide-6 chains were grafted on to Cloisite® 30B montmorillonite surface that had hydroxyl groups. Although the initial interlayer spacing of Cloisite® 15A is higher than that of Cloisite® 25A and 30B, no significant change was observed in the *d*-spacings of the nanocomposites with Cloisite® 15A. Exfoliation depends upon a variety of factors, such as, polymer–clay, polymer–surfactant, and clay–clay interactions, organoclay stability, and packing density, etc.[29] Among the other factors, here, it is observed that compatibility between the clay surface modifier and polymer matrix is essential to get an intercalated/exfoliated nanocomposite. According to suppliers' data, Cloisite® 15A has the most hydrophobic surface among the organoclays studied.[31] Also, it has no polar groups on its modifier. Polyamide-6 is a relatively polar polymer capable of making high degree of hydrogen bonding, and it also has a relatively good affinity for the polar surface of the montmorillonite.[32] Thus, it can be concluded that Cloisite® 15A is less compatible with polyamide-6 in comparison to the other two organoclays.

TEM analysis

TEM micrograph of polyamide-6 nanocomposite sample having no elastomer but 2 wt % Cloisite® 15A is shown in Figure 4(a). In the micrograph, the dark lines represent the thickness of individual clay layers or their agglomerates (tactoids), whereas the

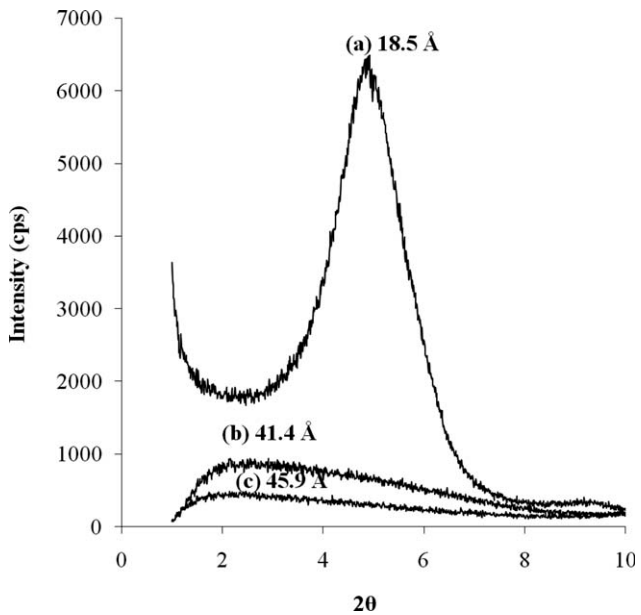

Figure 3 XRD patterns for (a) Cloisite® 30B, (b) polyamide-6/Cloisite® 30B nanocomposite, and (c) polyamide-6/Cloisite® 30B/E-MA-GMA nanocomposite.

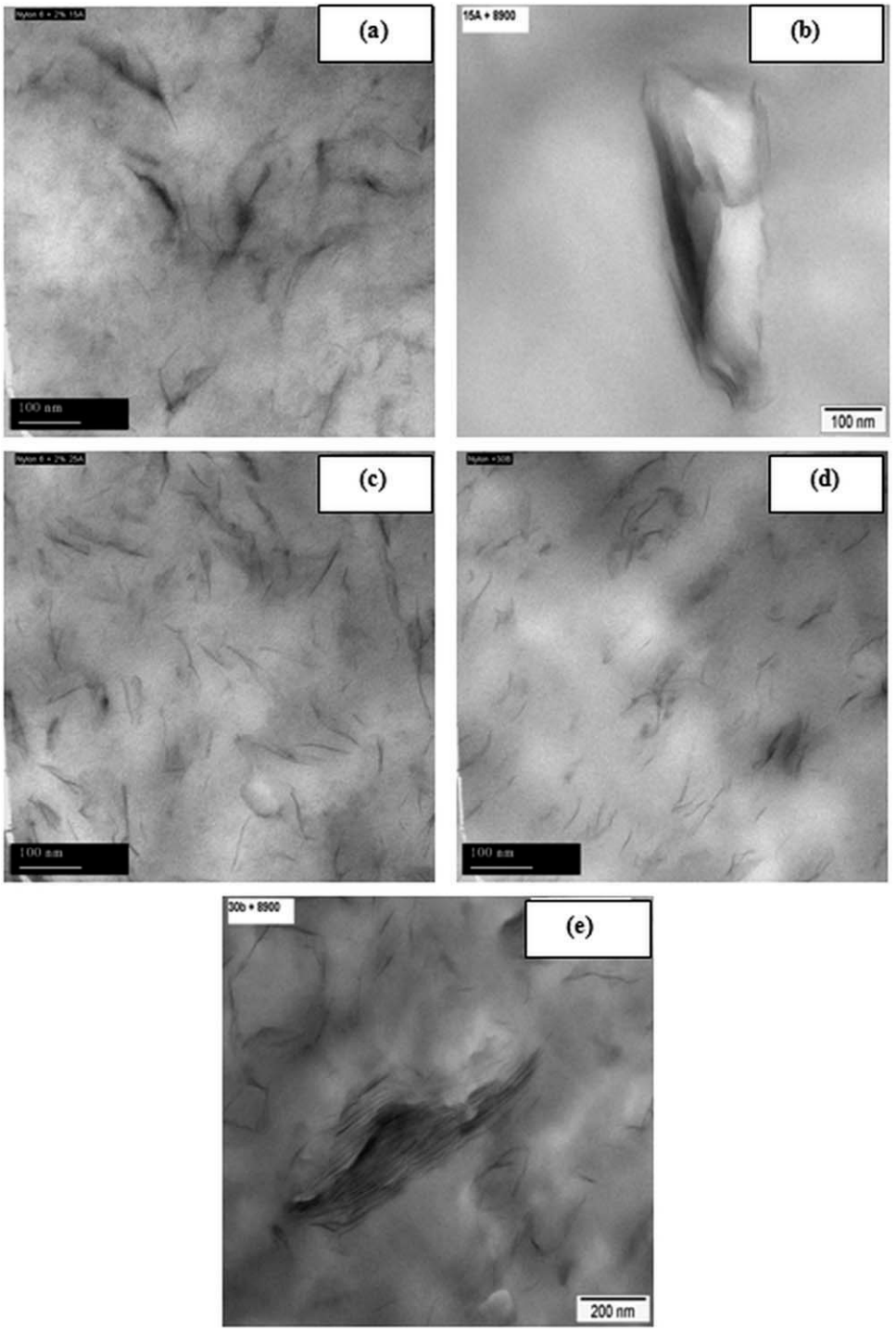

Figure 4 TEM micrographs of (a) polyamide-6/Cloisite® 15A nanocomposite, (b) polyamide-6/Cloisite® 15A/E-MA-GMA nanocomposite, (c) polyamide-6/Cloisite® 25A nanocomposite, (d) polyamide-6/Cloisite® 30B nanocomposite, and (e) polyamide-6/Cloisite® 30B/E-MA-GMA nanocomposite.

gray/white areas represent the polymer matrix. Several dark lines are observed indicating that stacked silicate layers are formed due to clustering and agglomeration. From XRD analysis it is observed that little change takes place in the *d*-spacing of Cloisite® 15A clay when it is melt blended with polyamide-6.

Figure 4(b) shows the TEM micrograph of polyamide-6/elastomer/organoclay ternary nanocomposite sample having 5 wt % E-MA-GMA and 2 wt % Cloisite® 15A. In the micrograph, stacked silicate layers can be seen as dark lines. The white dispersed domains correspond to the elastomeric phase. In agreement with the results reported by Baldi et al.[11]

and Khatua et al.,[15] clay platelets are not seen in the elastomer domains. Although a small amount of clay might be incorporated in the elastomer phase, it may be assumed that most of the platelets are contained in the polyamide-6 matrix. Rubber particles seem to affect the alignment of clay platelets in the nearby region. This finding is consistent with the XRD analysis since small change in *d*-spacing of pure Cloisite® 15A is observed in ternary nanocomposites composed of polyamide-6 and E-MA-GMA.

Figure 4(c) shows the TEM micrograph of polyamide-6 nanocomposite sample having 2 wt % Cloisite® 25A and no elastomer. The micrograph reveals that the organoclay is uniformly dispersed and exfoliated in the polyamide-6 matrix. The average thickness of clay appears to be just a few nanometers, whereas the average length is approximately 100 nm. From the XRD analysis, it is found that the characteristic clay diffraction peak for Cloisite® 25A is shifted to lower 2θ angles indicating intercalation. Thus, it can be concluded that polyamide-6/Cloisite® 25A nanocomposite has a partially exfoliated and partially intercalated structure.

Figure 4(d) shows the TEM micrograph of polyamide-6 nanocomposite sample having 2 wt % Cloisite® 30B and no elastomer. According to the micrograph, Cloisite® 30B is uniformly dispersed and exfoliated in polyamide-6 matrix. XRD analysis reveals that when Cloisite® 30B is melt blended with polyamide-6, a significantly intercalated structure is obtained. Thus, it can be concluded that polyamide-6/Cloisite® 30B nanocomposite has a mixed morphological structure, i.e., combination of intercalated stacks and exfoliated particles. If a comparison is made between Figure 4(a,c,d), it can be seen that degree of dispersion of Cloisite® 25A and 30B layers in polyamide-6 matrix is higher than the degree of dispersion of Cloisite® 15A layers in polyamide-6. The above observation is consistent with the XRD data and is attributed to the higher compatibility of these organoclays with the polymer matrix.

Figure 4(e) shows the TEM micrograph of polyamide-6/Cloisite® 30B/E-MA-GMA ternary nanocomposite sample. In the micrograph, both individual clay layers or their agglomerates (tactoids) and some stacked silicate layers, which are formed due to clustering, can be observed. The addition of elastomeric material hardly altered the dispersibility of organoclay 30B in the nanocomposites. The white dispersed domains in the micrograph correspond to the elastomer phase. Similar to Figure 4(b), clay platelets are not seen in the elastomer domains. Rubber particles seem to affect the alignment of the clay platelets in the nearby region. Organoclay 30B is observed to be partially exfoliated into a thinner multi-layered structure or even single layers in the micrographs. The thicknesses of the clay platelets in Figure 4(e) seem to be higher than in the polyamide-6/Cloisite® 30B nanocomposite with no elastomer. If Figure 4(d,e) are compared, it can be seen that the dispersibility of the organoclay is slightly altered with the addition of elastomeric material. The presence of reactively formed copolymer suppresses exfoliation in and near the interfacial area. Similar results were observed by Kelnar et al.[20]

SEM analysis

SEM analysis was performed to determine the size and the distribution of elastomer domains in the polymer matrix, since these factors, along with the interdomain distance, are very important parameters in toughening mechanism.

SEM micrographs of ternary nanocomposites in which E-MA-GMA elastomer is the dispersed phase are shown in Figure 5(a–d). The micrographs show two-phase, domain-in-matrix morphology. The rubber domain size data are summarized in Table III. Since the interfacial tension between the matrix and the dispersed phase might be changed in the presence of organoclay, rubber domain sizes are larger in the nanocomposites than in the polyamide-6/elastomer blend. Unless there is a large affinity between the matrix and organoclay, some organoclay particles might be located at the interphase, resulting in increase in the elastomer domain size.

It can be observed that the presence of the organoclay does not seem to substantially modify the dispersion of the rubber domains. This observation is unexpected, since higher viscosity of the nanocomposite matrix should lead to a lower dispersed phase size, considering that the rest of the parameters that would influence the domain size does not change. Ahn and Paul,[10] Baldi et al.,[11] and González et al.[18] observed results similar to the ones obtained in this study. The presence of organoclay helps coalescence of rubber domains. The increase in particle size is attributed to chemical and physical interactions between the organic modifier of the clay dissolved in the matrix and the functional groups of the elastomer, that would hinder the compatibilizing effect of the latter.

Polyamide-6 has reactive functionality through amine and carboxyl end groups that are capable of reacting to form graft moieties with the elastomer used. Previous studies demonstrated that both amines[33–35] and carboxylic acids[35,36] are capable of reacting with epoxide groups. In addition to these reactions, the epoxide group can also undergo ring-opening in the presence of acid, amine, and hydroxyl end groups.

The kinetics of epoxide ring reactions with amine and acid groups under melt processing conditions were studied by Kudva et al.[37] They concluded that

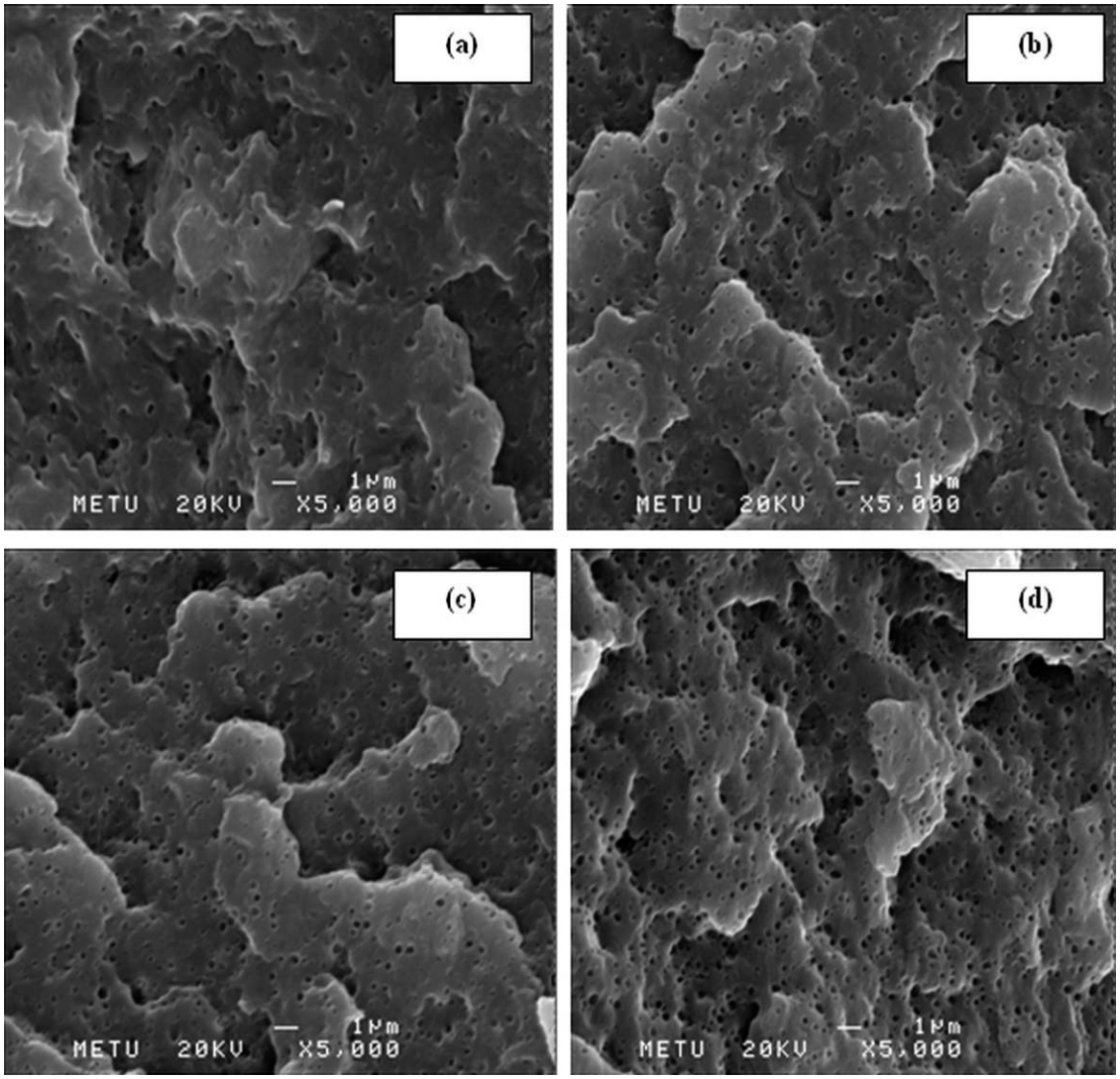

Figure 5 SEM micrographs of (a) polyamide-6/E-MA-GMA blend, (b) polyamide-6/Cloisite® 15A/E-MA-GMA nanocomposite, (c) polyamide-6/Cloisite® 25A/E-MA-GMA nanocomposite, (d) polyamide-6/Cloisite® 30B/E-MA-GMA nanocomposite.

these reactions take place easily and rapidly under melt blending conditions. Epoxy ring can react with hydroxyl functionalities. Reaction between the methyl acrylate functional groups and polyamide-6 is also possible. According to Akkapeddi,[38] reaction of ester group with polyamide-6 is very slow and can be negligible.

Effect of organoclay type on domain size of E-MA-GMA containing nanocomposites is shown in Table III. Different ion exchange capacities of the organoclays may also lead to different rubber domain sizes. Nanocomposite with Closite® 30B has the highest domain size. Among the organoclays used in this study, only Cloisite® 30B has reactive groups on its surfactant. Grafting reactions between E-MA-GMA/polyamide-6 and organoclay may lead to branching and crosslinking which may inhibit breakdown of rubber domains in the extruder.

MFI analysis

The MFI results of the nanocomposites prepared with polyamide-6, elastomer E-MA-GMA, and various organoclays are given in Table IV. The elastomer itself has a MFI of 14.6 ± 1.4 g/10 min ($T = 235°C$,

TABLE III
Elastomer E-MA-GMA Domain Size in Polyamide-6-Based Nanocomposites

	Domain size (nm)
Polyamide-6 + E-MA-GMA	85.4 ± 6.7
Polyamide-6 + Cloisite® 15A + E-MA-GMA	102.1 ± 6.4
Polyamide-6 + Cloisite® 25A + E-MA-GMA	99.0 ± 6.0
Polyamide-6 + Cloisite® 30B + E-MA-GMA	108.0 ± 6.6

TABLE IV
MFI (g/10 min) of the Materials Studied

	No clay	2 wt % Cloisite® 15A	2 wt % Cloisite® 25A	2 wt % Cloisite® 30B
Polyamide-6	34.3 ± 0.9	31.2 ± 0.2	35.3 ± 2.9	35.5 ± 3.4
Polyamide-6/E-MA-GMA	23.1 ± 0.5	24.9 ± 0.4	21.3 ± 0.2	25.7 ± 0.1

2.16 kg). It is seen from the table that, MFI of polyamide-6 decreases (viscosity increases) on addition of elastomer, owing to the high viscosity of elastomer and the possible reactions between functional groups of elastomer and polyamide-6.

In binary polyamide-6/organoclay nanocomposites, the addition of organoclay increases the MFI slightly (decreases the viscosity) in Cloisite® 25A and 30B organoclays as seen in Table IV. The increase in the viscosity value of the binary nanocomposite with Cloisite® 15A is basically due to large clusters formed by the organoclay. The decrease in the viscosity in binary nanocomposites with Cloisite® 25A and 30B can be attributed to higher clay platelet alignment and/or decrease of matrix molecular weight through degradation.[39] Increase in viscosity with rigid filler addition is balanced with the flow alignment of exfoliated clay and the polymer, which may cause an increase in MFI, hence decrease in dynamic viscosity. This is observed in case of Cloisite® 25A and 30B organoclays.

Mechanical properties

Figure 6 shows the variation in tensile strength with respect to both organoclay type and elastomeric material. As observed in this figure, in binary polyamide-6/organoclay nanocomposites, strength is increased with the addition of Cloisite® 25A and Cloisite® 30B organoclays with respect to unfilled polyamide-6. Clay organic modifier reduces the interlayer adhesion and promotes the compatibility with polyamide chains through interactions.

Hotta and Paul have shown that in polyamide-6 nanocomposites, one alkyl tail leads to much better dispersion of clay than do two tails.[40] They proposed that polyamide has relatively better affinity for the silicate surface than the alkyl part of organoclay. Thus, minimizing the number of alkyl tails maximizes platelet dispersion in this polar polymer.[40] The experimental data observed here lead to similar conclusions for the binary nanocomposites. Binary nanocomposites prepared with Cloisite® 25A and Cloisite® 30B (with one alkyl tail in each) have higher tensile strength and moduli in comparison to the binary nanocomposites prepared with Cloisite® 15A (with two alkyl tails).

For the organoclays 25A and 30B, XRD and TEM analysis results showed that the *d*-spacing of the organoclay is increased owing to the insertion of polyamide-6 matrix into clay galleries. This increase results in high contact surface area between the filler and the polymer matrix, thus tensile strength increases in binary nanocomposites with organoclays 25A and 30B. Cloisite® 15A decreases the tensile strength of polyamide-6 in this binary nanocomposite. Surfactant of this organoclay with no polar groups on its modifier has the most hydrophobic surface among the organoclays studied. Polyamide-6 is a relatively polar polymer which has capability of making high degree of hydrogen bonding, and has a relatively good affinity for the polar surface of the montmorillonite. Furthermore, it can be seen from Figure 1(b) that, *d*-spacing of pure Cloisite® 15A clay does not significantly change when it is melt blended with polyamide-6. For ternary nanocomposites, since the interactions between organoclay, elastomer, and polyamide-6 are very complex, it is difficult to comment on the effect of organoclay alkyl tail on mechanical properties.

Tensile strength of polyamide-6/organoclay binary nanocomposite decreases with the addition of E-MA-GMA, due to the lower tensile strength of the elastomer. Thus, it can be concluded that, at these concentrations, the effect of elastomer on tensile strength is more dominant than the effect of organoclay. Tensile strengths in Cloisite® 15A and 25A containing ternary nanocomposites are nearly the same,

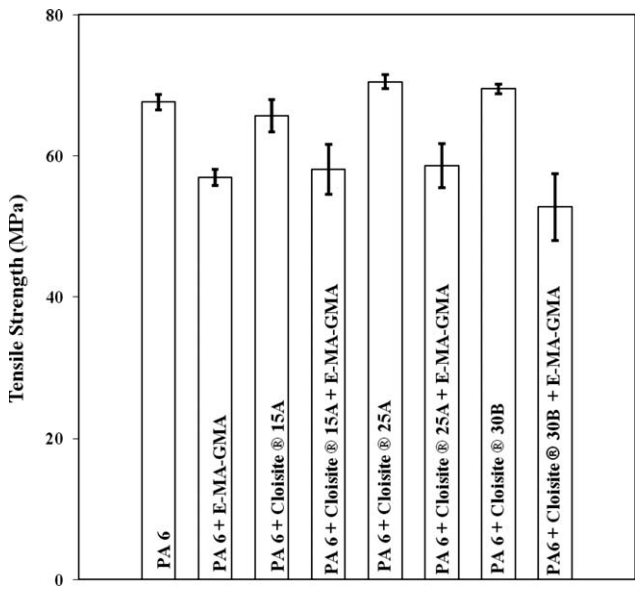

Figure 6 Effect of organoclay type on tensile strength of rubber toughened polyamide-6 nanocomposites.

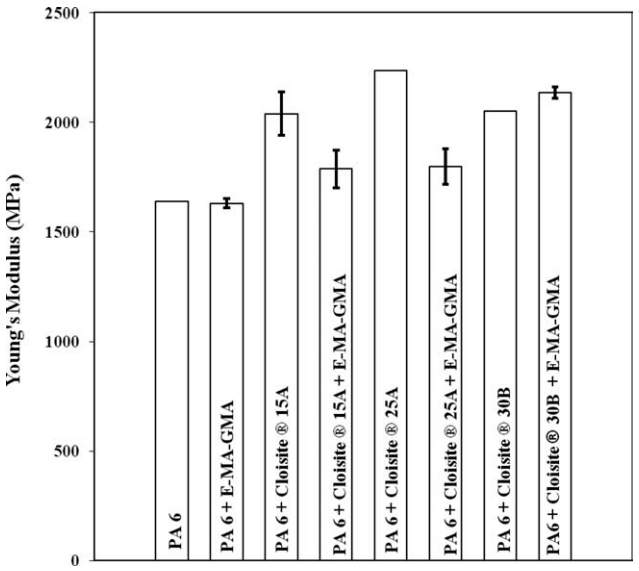

Figure 7 Effect of organoclay type on Young's modulus of rubber toughened polyamide-6 nanocomposites.

and they are higher than the tensile strength of Cloisite®30B containing nanocomposites.

Figure 7 shows the variation in Young's modulus with respect to both organoclay type and elastomeric material. Experimental results indicate that in the polyamide-6/elastomer blend, Young's modulus remain unchanged with respect to the Young's modulus of polyamide-6, due to the low amount of elastomer and possible chain extension/branching reactions that may have occurred. The Young's moduli of binary nanocomposites are higher than the modulus of neat polyamide-6. The increase in modulus indicates a decrease in molecular mobility that may be the result of large interphase area/dispersed phase volume ratio, characteristic of intercalated/exfoliated nanocomposites. In ternary systems composed of polyamide-6, organoclay, and elastomer, except for the Cloisite® 30B containing ternary nanocomposite, Young's modulus decreases when compared to binary nanocomposites with no elastomer. Polyamide-6/Cloisite® 30B/E-MA-GMA nanocomposite has the highest modulus among the other ternary nanocomposites, since there would be high possibility of interactions between polyamide-6, E-MA-GMA, and the —OH groups of clay surfactant.

Figure 8 shows the variation in elongation at break with respect to both organoclay type and elastomer. As it can be seen in the figure, elongation at break decreases with the addition of elastomer E-MA-GMA. Two main reasons can be invoked to explain the reduction of elongation at break for the blends: (1) GMA can react with both amine and acidic end groups of polyamide-6. Owing to these reactions and the presence of methyl acrylate groups, ternary composites become less capable of extending, thus the strain at break decreases. (2) It may be attributed to the hindrance effect of free elastomer domains to cold drawing and the copolymer network effect which makes the polymer matrix more or less interconnected, therefore less capable of extending. Elongation at break values of the binary nanocomposite samples are higher than that of unmodified polyamide-6. Generally, rigid inorganic particles decrease the elongation at break when their size is rather large. The organoclays used in this study increase the elongation at break by acting as crack stoppers.

Impact strengths of polyamide 6-elastomer blend, nanocomposites, and ternary systems can be seen in Figure 9. Addition of organoclay decreases the impact strength, whereas elastomer incorporation to polyamide-6 and binary nanocomposites increases the impact strength. All ternary nanocomposites give nearly the same impact strength, which is higher than the impact strengths of their corresponding binary nanocomposites. SEM micrographs show that the elastomer forms a second phase in the polymer matrix. The rubber particles act as stress concentrators in producing crazes. A very large surface area is produced during the crazing and dewetting processes, thus high energy can be absorbed. Reactions occurring between polyamide-6 and elastomer are also important, since there would be strong adhesion between the polyamide-6 and elastomer.

Although the TEM micrographs in Figure 4(d,e) show that the elastomer domains suppress the dispersion of clay in the polymer matrix, impact strength increases in ternary nanocomposites. It can be concluded that, for the concentrations used, the effect of elastomer is more dominant than the effect

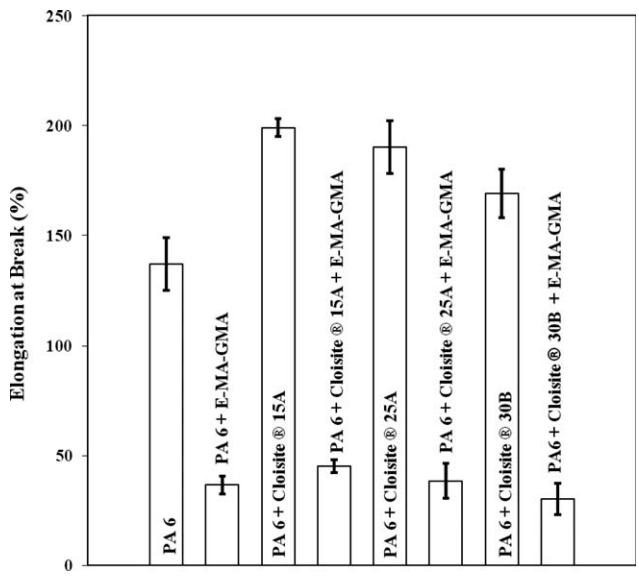

Figure 8 Effect of organoclay type on elongation at break of rubber toughened polyamide-6 nanocomposites.

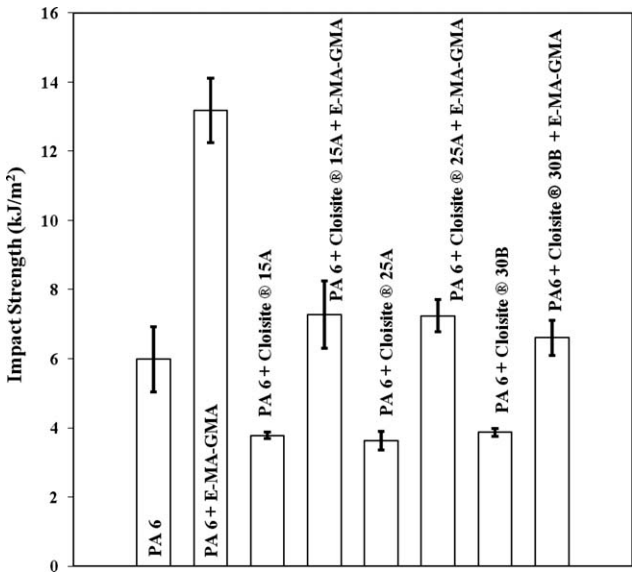

Figure 9 Effect of organoclay type on impact strength of rubber toughened polyamide-6 nanocomposites.

of organoclay in terms of impact strength, as it is also observed for the tensile strength.

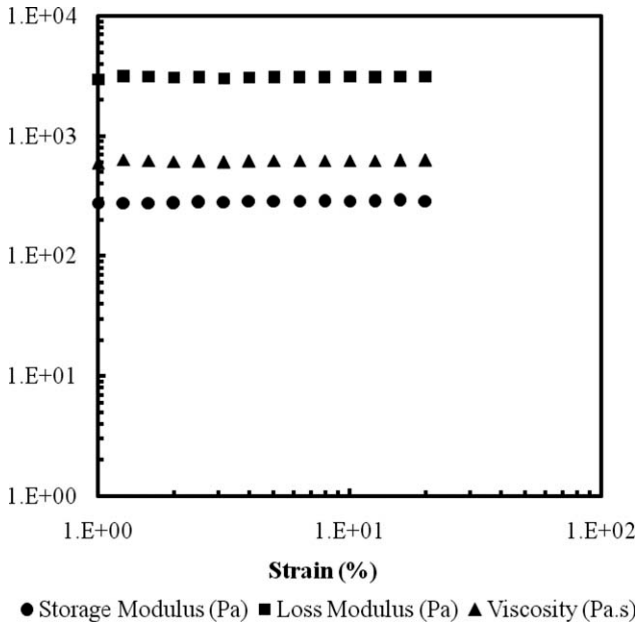

Figure 10 Effect of strain amplitude on viscoelastic properties of polyamide-6/Cloisite® 25A/E-MA-GMA nanocomposite in the melt state.

Dynamic rheological analysis

Figure 10 shows logarithmic plots of storage modulus, loss modulus, and complex viscosity versus percentage strain amplitude for the polyamide-6/Cloisite® 25A/E-MA-GMA nanocomposite, at 240°C and 5 rad/s angular frequency, obtained by using parallel disk oscillating rheometer. Storage and loss moduli, as well as complex viscosity remain constant in 1–20% amplitude range. Thus, in the analysis that followed 5% strain amplitude was selected to ensure that the experiments are performed in the linear viscoelastic region.

The storage and loss moduli and complex viscosity resulting from dynamic frequency scans for polyamide-6/organoclay/E-MA-GMA nanocomposites are shown in Figures 11–13.

Both storage and loss moduli and complex viscosity of unfilled polyamide-6 increase with organoclay in the frequency range studied. This reflects the strong effect of intercalated/exfoliated clay layers on the viscosity of polyamide-6. Increase in complex viscosity is higher in binary polyamide-6/Cloisite® 15A nanocomposites than in polyamide-6/Cloisite® 25A and polyamide-6/Cloisite® 30B binary nanocomposites, as also observed in the MFI analysis in Table IV. This strongly supports the hypothesis that flow alignment of exfoliated clay and the polymer, shown in TEM Figure 4(a,c,d), affects the complex viscosity. The degree of dispersion of Cloisite® 25A and 30B layers in polyamide-6 matrix is higher than the degree of dispersion of Cloisite® 15A layers in

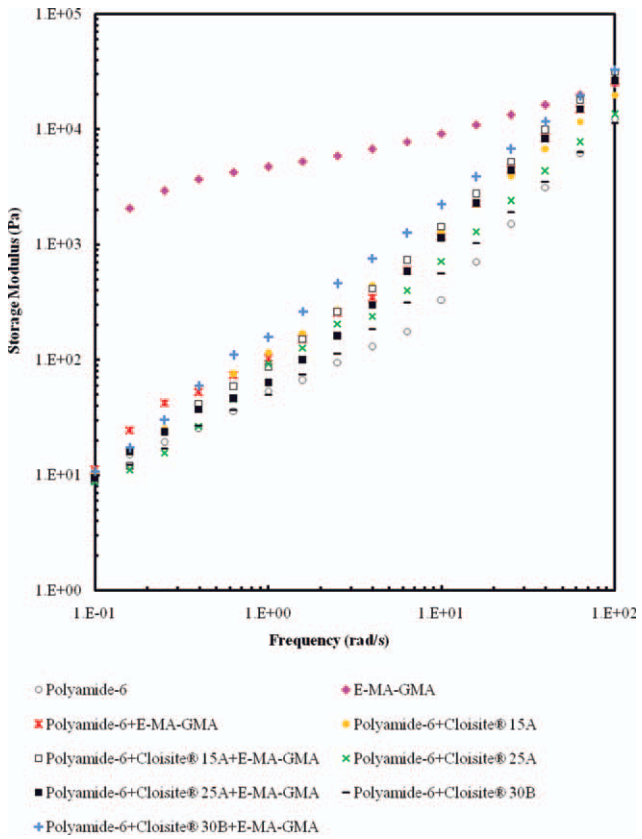

Figure 11 Effect of frequency on storage modulus for rubber toughened polyamide-6/organoclay nanocomposites. [Color figure can be viewed in the online issue, which is available at wileyonlinelibrary.com.]

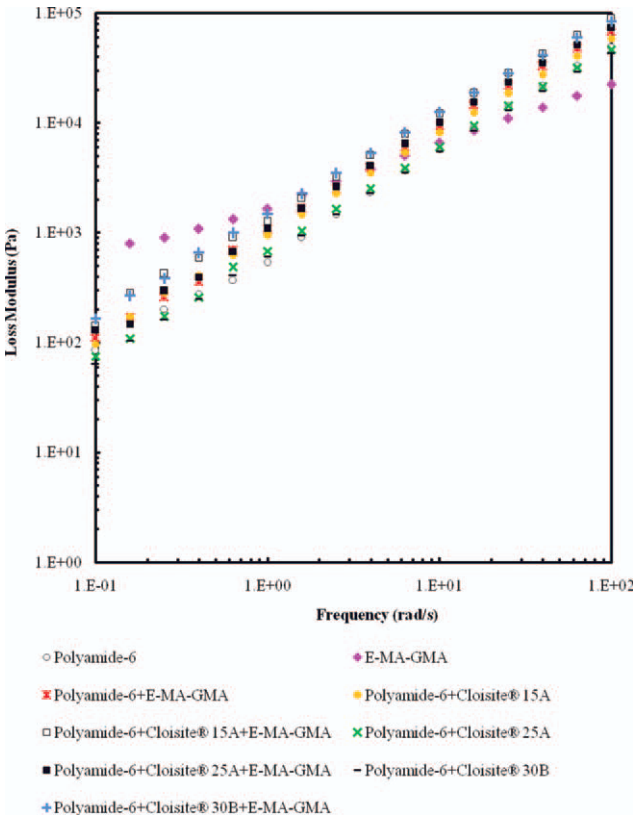

Figure 12 Effect of frequency on loss modulus for rubber toughened polyamide-6/organoclay nanocomposites. [Color figure can be viewed in the online issue, which is available at wileyonlinelibrary.com.]

polyamide-6. If the clay layers are exfoliated, shear thinning is more probable than in the case of intercalated tactoids. Shear thinning assumes an alignment of the clay layers in the flow direction, which occurs easily in the exfoliated stage.[15] This observation is consistent with the XRD data shown in Figures 1–3 and is attributed to the higher compatibility of Cloisite® 25A and 30B with the polymer matrix.

Elastomer E-MA-GMA exhibits pseudo solid-like non-Newtonian behavior, since the complex viscosity increases strongly with decreasing frequency. In contrast, polyamide-6-based blend and nanocomposites reveal Newtonian-like behavior, since complex viscosity is not significantly changed with frequency at low frequencies. Incorporation of E-MA-GMA elastomer increases the complex viscosity of unfilled polyamide-6 and binary nanocomposites in the viscoelastic range studied. This is due to the high viscosity of elastomer E-MA-GMA and the reactions occurring between polyamide-6 and E-MA-GMA which lead to the formation of graft copolymers. MFI results in Table IV support the observations made here. Complex viscosities of polyamide-6/organoclay/E-MA-GMA ternary nanocomposites are generally higher than those of polyamide-6/E-MA-GMA blends owing to the flow hindrance by organoclay particles and interactions between organoclay and polyamide-6.[15] In addition to these, TEM micrographs in Figure 4(d,e) show that organoclay dispersibility is altered with the addition of elastomer. The presence of reactively formed copolymer suppresses exfoliation in and near the interfacial area. Thus, complex viscosities increase. Complex viscosity of polyamide-6/Cloisite® 30B/E-MA-GMA nanocomposite is higher than the complex viscosity of other ternary nanocomposites, since the interactions between organoclay —OH groups in 30B and GMA lead to an increase in viscosity.

Cole–Cole plot in Figure 14 shows the relationship between the loss and storage moduli. The dashed line in the figure represents $G'' = G'$. It is seen that the elastomer E-MA-GMA is more elastic than polyamide-6 and nanocomposites, since it is on the right side of the equi-moduli line. Loss moduli of polyamide-6-based nanocomposites are greater than the storage moduli throughout the frequency range. Liquid-like behavior of polyamide-6 slightly turns to pseudo solid-like in the binary and ternary nanocomposites. Solid-like behavior is attributed to the formation of a percolated network superstructure of the exfoliated layers or stacks of intercalated layers.[23]

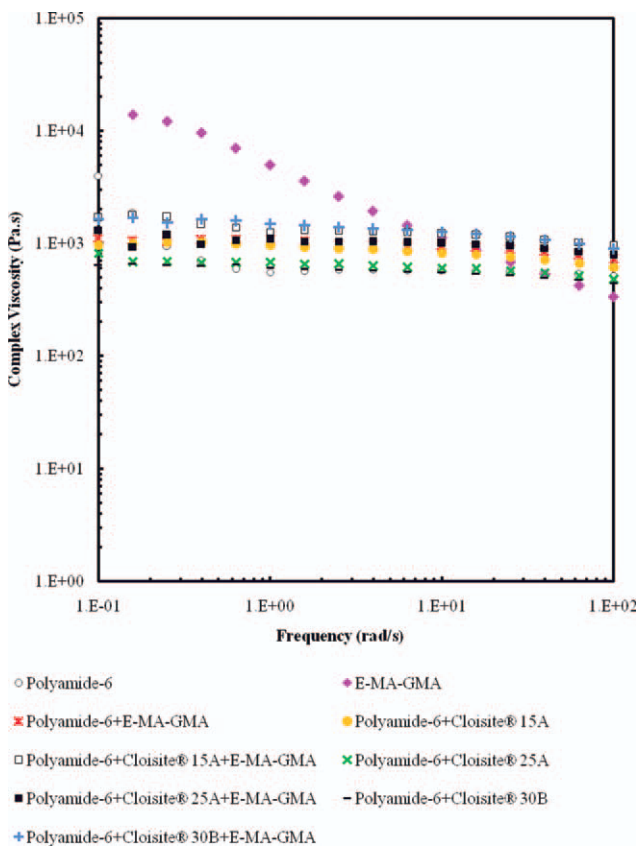

Figure 13 Effect of frequency on complex viscosity for rubber toughened polyamide-6/organoclay nanocomposites. [Color figure can be viewed in the online issue, which is available at wileyonlinelibrary.com.]

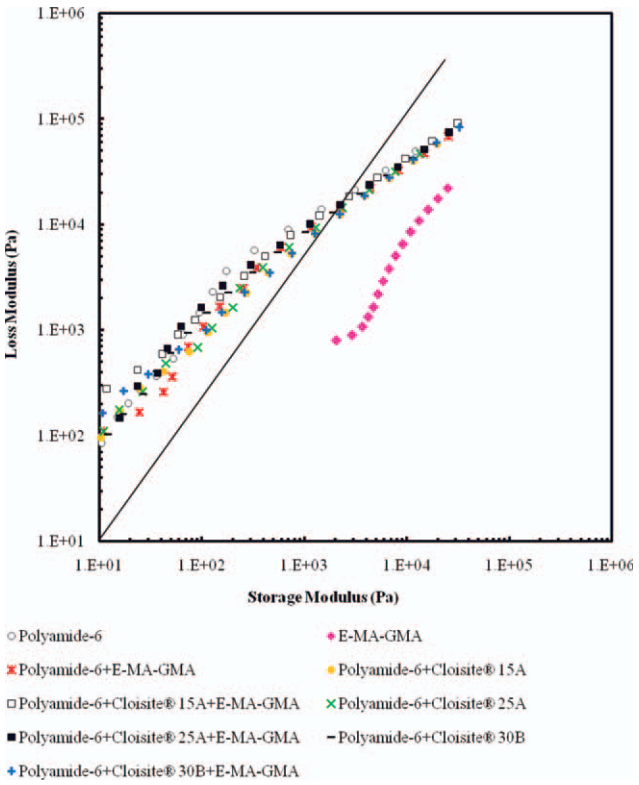

Figure 14 Loss modulus as a function of storage modulus for rubber toughened polyamide-6/organoclay nanocomposites. [Color figure can be viewed in the online issue, which is available at wileyonlinelibrary.com.]

CONCLUSIONS

Original d_{001} *d*-spacing of organoclay Cloisite® 15A was not significantly changed in binary as well as ternary nanocomposite systems, whereas d_2 peak was shifted to lower angles when organoclay 15A was compounded with polymers indicating that a few polymer chains are intercalated between the clay layers. XRD patterns showed that the interlayer spacing of the organoclays Cloisite® 25A and Cloisite® 30B increased in both polyamide-6/organoclay binary nanocomposites and in ternary systems. TEM analysis showed that exfoliated-intercalated nanocomposites were formed. In ternary nanocomposites, clay platelets were not seen in the elastomer domains, and the rubber domains affected the alignment of clay platelets in the nearby region.

SEM micrographs of the binary blends and ternary nanocomposites showed two-phase, particle-in-matrix morphology. Rubber domain sizes were larger in nanocomposites than in their corresponding polyamide-6/elastomer blends.

Tensile strength increased in binary polyamide-6/organoclay nanocomposites with the addition of Cloisite® 25A and Cloisite® 30B. Thus, Young's moduli of these binary nanocomposites increased with respect to that of unfilled polyamide-6. All the organoclays increased the elongation at break of polyamide-6 by acting as crack stoppers. In ternary nanocomposites, the effect of elastomer was more dominant than the effect of organoclay in terms of tensile strength. Tensile strengths of Cloisite® 15A and 25A containing ternary nanocomposites were nearly the same and they were higher than the tensile strength of Cloisite® 30B containing nanocomposites.

All ternary nanocomposites had nearly the same impact strength, which was higher than the impact strengths of their corresponding binary nanocomposites. It was seen that incorporation of elastomeric material increased the impact strength, whereas in binary nanocomposites the addition of organoclay only decreased the impact strength.

Addition of Cloisite® 15A to polyamide-6 decreased the MFI, whereas the addition of Cloisite® 25A or 30B to polyamide-6 increased the MFI of the base polymer. MFI of polyamide-6 decreased on addition of elastomer. In the ternary nanocomposites, generally, the addition of clay led to an increase in MFI with respect to the MFI of the polyamide-6/elastomer blends.

In the melt state, polyamide-6-based blends and nanocomposites exhibited Newtonian-like behavior. Incorporation of E-MA-GMA elastomer increased the complex viscosity of unfilled polyamide-6 and binary nanocomposites. In the melt state, the increase in storage modulus, loss modulus, and complex viscosity were higher in binary polyamide-6/Cloisite® 15A nanocomposites than in polyamide-6/Cloisite® 25A and polyamide-6/Cloisite® 30B binary nanocomposites, owing to high organoclay surface–surface interactions.

Polyamide-6/Cloisite® 30B/E-MA-GMA ternary nanocomposite had the highest Young's modulus, complex viscosity, and storage modulus values among the ternary nanocomposites, since there exists high potential of interactions between polyamide-6, E-MA-GMA, and the —OH groups of clay surfactant.

References

1. Kojima, Y.; Usuki, A.; Kawasumi, M.; Okada, A.; Kurauchi, T.; Kamigaito, O. J Polym Sci Part A: Polym Chem 1993, 31, 983.
2. Kojima, Y.; Usuki, A.; Kawasumi, M.; Okada, A.; Kurauchi, T.; Kamigaito, O.; Kaji, K. J Polym Sci Part B: Polym Phys 1994, 32, 625.
3. Usuki, A.; Koiwai, A.; Kojima, Y.; Kawasumi, M.; Okada, A.; Kurauchi, T.; Kamigaito, O. J Appl Polym Sci 1995, 55, 119.
4. Cho, J. W.; Paul, D. R. Polymer 2001, 42, 1083.
5. Kusmono; MohdIshak, Z. A.; Chow, W. S.; Takeichi, T.; Rochmadi. Eur Polym J 2008, 44, 1023.
6. Kusmono; MohdIshak, Z. A.; Chow, W. S.; Takeichi, T.; Rochmadi. Compos A 2008, 39, 1802.
7. Dayma, N.; Satapathy, B. K. Mater Design 2010, 31, 4693.

8. Liu, X.; Wu, Q.; Berglund, L. A.; Fan, J.; Qi, Z. Polymer 2001, 42, 8235.
9. Tjong, S. C.; Bao, S. P. J Polym Sci Part B: Polym Phys 2005, 43, 585.
10. Ahn, Y. C.; Paul, D. R. Polymer 2006, 47, 2830.
11. Baldi, F.; Bignotti, F.; Tieghi, G.; Ricco, T. J Appl Polym Sci 2006, 99, 3406.
12. Chow, W. S.; MohdIshak, Z. A.; Karger-Kocsis, J.; Apostolov, A. A.; Ishiaku, U. S. Polymer 2003, 44, 7427.
13. Chow, W. S.; Mohd Ihsak, Z. A.; Ishiaku, U. S.; Karger-Kocsis, J.; Apostolov, A. A. J Appl Polym Sci 2004, 91, 175.
14. Chow, W. S.; MohdIhsak, Z. A.; Karger-Kocsis, J. Macromol Mater Eng 2005, 290, 122.
15. Khatua, B. B.; Lee, D. J.; Kim, H. Y.; Kim, J. K. Macromolecules 2004, 37, 2454.
16. Chiu, F. C.; Lai, S. M.; Chen, Y. L.; Lee, T. H. Polymer 2005, 46, 11600.
17. González, I.; Eguiazábal, J. I.; Nazábal, J. Compos Sci Technol 2006, 66, 1833.
18. González, I.; Eguiazábal, J. I.; Nazábal, J. Eur Polym J 2006, 42, 2905.
19. Nishitani, Y.; Yamada, Y.; Ishii, C.; Sekiguchi, I.; Kitano, T. Polym Eng Sci 2010, 50, 100.
20. Kelnar, I.; Kotek, J.; Kaprálková, L.; Hromádková, J.; Kratochvíl, J. J Appl Polym Sci 2006, 100, 1571.
21. Kelnar, I.; Khunová, V.; Kotek, J.; Kaprálková, L. Polymer 2007, 48, 5332.
22. Krishnamoorti, R.; Vaia, R.; Giannelis, E. P. Chem Mater 1996, 8, 1728.
23. Krishnamoorti, R.; Yurekli, K. Curr Opin Colloid Interface Sci 2001, 6, 464.
24. Krishnamoorti, R.; Giannelis, E. P. Macromolecules 1997, 30, 4097.
25. Taghizadeh, E.; Naderi, G.; Dubois, C. Rheol Acta 2010, 49, 1015.
26. Mehrabzadeh, M.; Kamal, M. Polym Eng Sci 2004, 44, 1151.
27. Finnigan, B.; Martin, D.; Halley, P.; Truss, R.; Campell, K. J Appl Polym Sci 2005, 97, 300.
28. Mert, M.; Yilmazer, U. Adv Polym Technol 2009, 28, 155.
29. Lee, M. H.; Dan, C. H.; Kim, J. H.; Cha, J.; Kim, S.; Hwang, Y.; Lee, C. H. Polymer 2005, 47, 4359.
30. Mohamadi, S.; Sanjani, N. S.; Qazvini, N. T.; Mohammad, B. M. J Nanosci Nanotechnol 2009, 9, 3959.
31. Cloisite® Selection Chart Based on Polymer/Monomer Chemistry 2011, Retrieved December 20, 2011 from http://www.nanoclay.com/selection_chart.asp#
32. Fornes, T. D.; Yoona, P. J.; Hunterb, D. L.; Keskkula, H.; Paul, D. R. Polymer 2002, 43, 5915.
33. Duffy, J. V.; Hui, E.; Hartmann, B. J Appl Polym Sci 1987, 33, 2959.
34. Glover, D. J.; Duffy, J. V.; Hartmann, B. J Polym Sci Part A: Polym Chem 1988, 26, 79.
35. Kalal, J.; Svec, F.; Marousek, V. J Polym Sci Part C: Polym Symp 1974, 47, 155.
36. Shechter, L.; Wynstra, J. Ind Eng Chem 1956, 48, 86.
37. Kudva, R. A.; Keskkula, H.; Paul, D.R. Polymer 1998, 39, 2447.
38. Akkapeddi, M. K. In Reactive Polymer Blending; Baker, W.; Scott, C.; Hu, G. H., Eds.; Hanser Gardner Publications, Inc.: USA, 2001; pp 207–253.
39. Fornes, T. D.; Yoon, P. J.; Keskkula, H.; Paul, D. R. Polymer 2001, 42, 9929.
40. Hotta, S.; Paul, D. R. Polymer 2004, 45, 7639.